

pubs.acs.org/acschemicalbiology Article

De Novo Synthesis and Structural Elucidation of CDR-H3 Loop Mimics

Guangkuan Zhao, Alexis D. Richaud, R. Thomas Williamson, Michael Feig,* and Stéphane P. Roche*



Cite This: ACS Chem. Biol. 2024, 19, 1583–1592



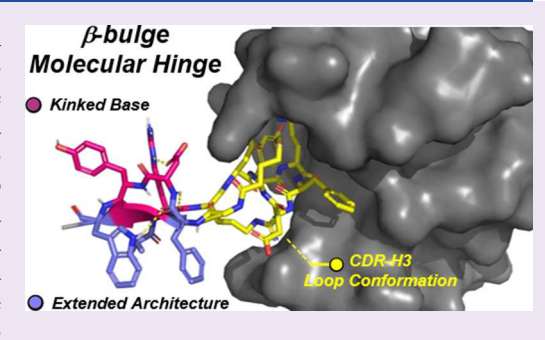
ACCESS

III Metrics & More

Article Recommendations

SI Supporting Information

ABSTRACT: The binding affinity of antibodies to specific antigens stems from a remarkably broad repertoire of hypervariable loops known as complementarity-determining regions (CDRs). While recognizing the pivotal role of the heavy-chain 3 CDRs (CDR-H3s) in maximizing antibody—antigen affinity and specificity, the key structural determinants responsible for their adaptability to diverse loop sequences, lengths, and noncanonical structures are hitherto unknown. To address this question, we achieved a de novo synthesis of bulged CDR-H3 mimics excised from their full antibody context. CD and NMR data revealed that these stable standalone β -hairpin scaffolds are well-folded and retain many of the native bulge CDR-H3 features in water. In particular, the tryptophan residue, highly conserved across CDR-H3 sequences, was found to



extend the kinked base of these β -bulges through a combination of stabilizing intramolecular hydrogen bond and CH/ π interaction. The structural ensemble consistent with our NMR observations exposed the dynamic nature of residues at the base of the loop, suggesting that β -bulges act as molecular hinges connecting the rigid stem to the more flexible loops of CDR-H3s. We anticipate that this deeper structural understanding of CDR-H3s will lay the foundation to inform the design of antibody drugs broadly and engineer novel CDR-H3 peptide scaffolds as therapeutics.

■ INTRODUCTION

Following an infection, repeated cycles of antigen-binding affinity selection accelerate the production of B cells to express a large repertoire of primary antibodies (Abs). These antibodies share a central core structure wrapped around a constant and a variable region that combines a heavy and a light chain (H, L respectively) each being composed of three CDRs tipped by functional loops essential to maximize the antigen-binding affinity (paratope). The initial Ab germline selection usually requires high levels of promiscuity and flexibility within the paratope center (L3/H3 loops). One of the current hypotheses is on how extensive the repertoire of antibodies can be generated via germline and somatic selection relies markedly on the mechanisms controlling the CDR-H3 diversity. Upon successive exposure to the same antigen, the affinity-driven selection results in the rigidification of CDRs to procure antibodies with an exquisite antigenbinding affinity.⁴⁻⁶ Although still debated,^{7,8} this mechanism has been proposed to be intimately associated with the rigidification of CDR-H3s, 5,9-12 thus raising questions about the origin and the relationship between H3 loops' binding affinity and their conformational adaptivity upon binding.

While each of the CDR-L1-3 and H1-2 structures can be entirely defined into distinct canonical ensembles, ¹³⁻¹⁵ the relationship between the primary amino acid sequences of CDR-H3s and their 3D-structures has remained unclear for over 20 years. CDR-H3s are indeed known to possess an extraordinary variability of primary sequences^{2,3,16} and

lengths¹⁷ which drastically increases the conformational space sampled by their loops ^{18,19} and their ability to access binding-competent conformations. ^{5,10,20,21} For example, a remarkable CDR-H3 loop conformational switch resulting in a drastic *cis-trans* proline isomerization was recently characterized in the course of antibody 9E5 response to antigen binding. ²² Along these lines, it was shown that H3 loops are typically accountable for \sim 30% of the entire antibody paratope surface (out of six loops)²³ and possess innate dynamic properties to maximize conformational selection geared toward antigen binding. ^{24–26} Given the unsolved challenge posed by H3 loops for computational modeling, there is currently no way to systematically and accurately predict their 3D-structural ensembles to assist the rational design of antibody drugs. ^{27–31}

The vast majority of CDR-H3s possess an irregular bulged β -structure flanking both loop termini that causes the variable loops to protrude in a kinked manner.^{32–34} However, the role played by this motif in the CDR nucleation and/or in its thermodynamic stability remains practically unexplored. One

Received: April 5, 2024 Revised: May 31, 2024 Accepted: June 10, 2024 Published: June 25, 2024





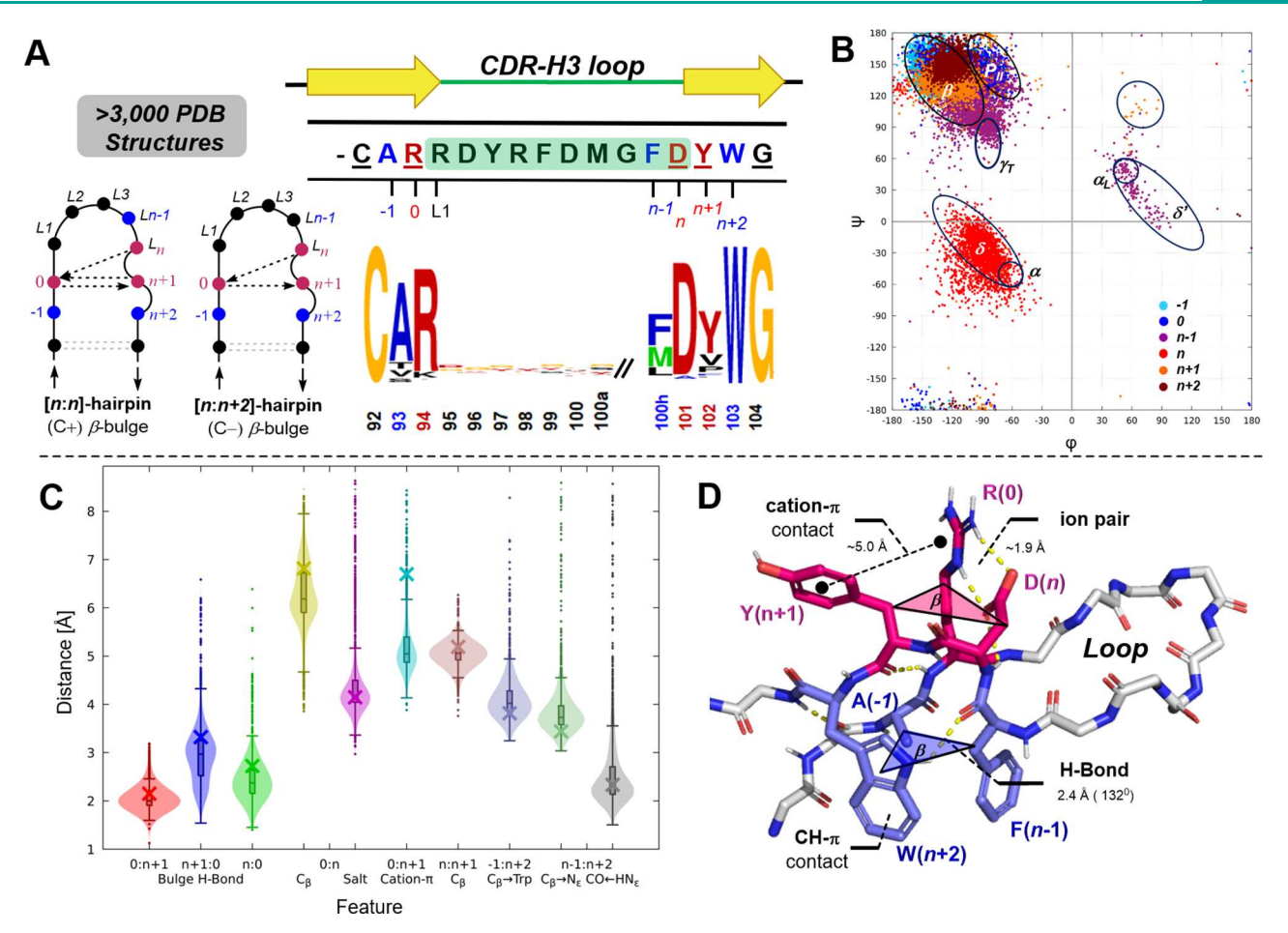


Figure 1. Structural and conformational analysis of extended β -bulges edging CDR-H3 loops from PDB structures. (A) Schematic representation of (C+/C-) β -bulge types based on H-bond patterns between the loop and stem segments of CDR-H3s (SI, Figure S1); Introducing a general numbering notation $A^{-1}\underline{R}^{0}\cdots F^{n-1}\underline{D}^{n}\underline{X}^{n+1}W^{n+2}$ for any 6-residue extended bulge sequence and logo plot representing the sequence diversity of bulged CDR-H3s. (B) Ramachandran analysis of bulged CDR-H3 structures with backbone φ/ψ torsion angles highlighting the conformational diversity and the noncanonical space sampled at positions n-1 (mauve) and n (red). Data is shown for all clusters with YCARx.xDYWGQ consensus sequences. (C) Violin plot presenting the distribution of structural features for CDR-H3 bulge residues. Boxes indicate first quartile, median, and third quartile. Whiskers identify data outside the central quarters within 1.5 times the interquartile range. Pembrolizumab values indicated with 'x' marks. (D) Working hypothesis based on proposed noncovalent interactions within CDR-H3 β -bulges; Characteristic features include: A(-1):W(n+2) CH/ π and Y(n+1):R(0) cation- π interactions, R(0):D(n) ionic pair, and a W(n+2):F(n+1) intramolecular H-bond shown on the prototypical bulged CDR-H3 of pembrolizumab (PBD: SB8C).

could imagine that the promiscuity of bulged H3 loops among all CDR-H3s is not a result of accidental misfolding but instead has been evolutionary optimized to favor the display of a large repertoire of 3D-structures that can conformationally adapt and rigidify to achieve an optimum Ag binding pose. Guided by the bioinformatics analysis of known CDR-H3 like structures, we synthesized an archetypal CDR-H3 bulge motif —AR···FD YW— excised from the pembrolizumab antibody (Protein Data Bank (PDB) code: 5B8C) into standalone β -hairpin mimics and determined their innate stability. To obtain stable CDR-H3 structures, variations of the original sequence 1a were evaluated. We determined the unique spectral signature of this motif by CD (circular dichroism) and NMR (nuclear magnetic resonance) spectroscopy combined with computational analysis. The strong correlation observed between the thermal denaturation curves (CD-melts) of the bulge motif and the entire hairpin strongly suggests that bulges afford additional stabilization to the global hairpin fold in comparison to a regular β -hairpin. In addition, the NMR-generated conformational ensemble of the H3 β hairpin mimic 1d revealed that many of the key features

present in CDR-H3 crystal structures are present in the free-state solution structure. This suggests that the intact antibody framework is not essential in stabilizing the CDR-H3 motif and that synthetic CDR-H3 mimics can be studied for the first time outside of their full antibody context. The distinctive features presented herein provide important insights for crafting bioactive peptides into novel and stable CDR-H3 scaffolds and ultimately inform the design of antibody drugs broadly.

RESULTS AND DISCUSSION

Identification of β -Bulge Consensus Sequences and Structural Variations from PDB Structures and Their Occurrence in CDR-H3s. Although β -bulges are relatively common secondary structures (avg. 2.5 per protein), $^{35-37}$ they are usually considered as simple strand misalignment irregularities. 38,39 As originally described by Nakamura over 25 years ago, 32 most antibody CDR-H3s (n-residue long loop) possess a G1 bulged "torso" domain wrapped around a prototypical three-residue bulge sequence $\underline{\mathbf{R}}_0 \cdots \underline{\mathbf{D}}_n \underline{\mathbf{Y}}_{n+1}$ (magenta in Figure 1) featuring a salt bridge $\mathbf{R}^+(0):\mathbf{D}^-(n)$ as the

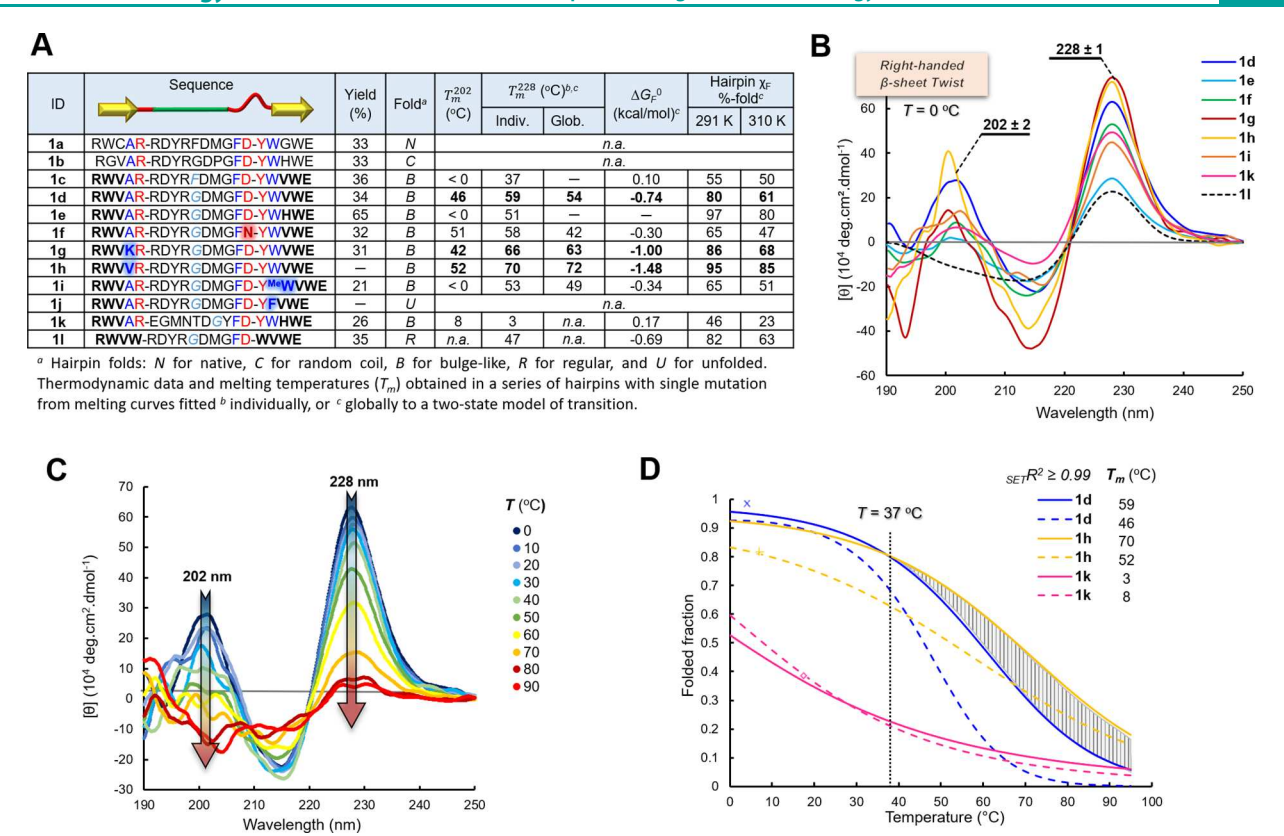


Figure 2. Characterization of the β-hairpin tertiary structures and a kinked bulge-like motif signature by CD spectroscopy. (A) Synthetic library of CDR-H3 peptide mimics; Synthetic yields and thermodynamic folding properties of β-hairpins obtained by CD analysis are reported. (B) Overlay of CD spectra obtained at 0 °C between a regular benchmark hairpin 11 and the novel bulge-like hairpins 1d-k: typical exciton couplet for a W/W pair at the hairpin strap termini (228 ± 1 nm) and a novel CD band attributed to the bulge-like structure (202 ± 2 nm). (C) Representative thermal denaturation of hairpin 1d monitored at both 202 and 228 nm. (D) Comparison between individual best-fitted melting curves for selected hairpins 1d,h,k based on a two-state model (global hairpin fraying vs local kinked motif denaturation in solid and dashed lines respectively).

key structuring element and a distinctive side-chain hydrogen bond between the W(n + 2) NH^{$\epsilon 1$} and the backbone carbonyl of F(n-1). Given the increasingly large number of highresolution crystal structures (res ≤ 2.5 Å), in the PDB, we decided to take a more comprehensive view of G1 bulge motifs. A structure-based search extracted a broad range of antibody, nanobody, and nonantibody protein structures with nonredundant sequences (>90%) containing the characteristic forked hydrogen bond network of bulges with loops of varying lengths (Figure 1A). While β -bulge motifs were found with a wide variety of sequences, the highest level of sequence and structure conservation was found for CDR-H3 loops with a consensus sequence pattern of YCAR-loop-D YWGQ. Residues CH92 and GH104 (with corresponding Kabat numbering) represent the start and end of CDR-H3 motifs with residues forming the typical β -bulge base underlined.

We subsequently focused our analysis on structural motifs extracted from the PDB (in March 2021) with a sequence similar to the consensus with 4 to 20 residue-long loops (see SI for details). In this analysis, even identical consensus sequences were considered to capture most loop and bulge structural variations. As a result, we identified about 3283 structural fragments matching the consensus sequence pattern. As introduced previously by Gray, 29,40 a τ_{101} vs α_{101} angle plot was used to distinguish loops with bulges found in a kinked orientation to those of regular hairpins (Figure S1). Out of the entire set, 2377 structures had bulge-like features, whereas the remaining structures mostly consisted of regular hairpins. The

loop length distribution in the structures with bulges was consistent to earlier reports on CDR-H3s with a mean length of 11.4 AAs (Figure S2).2 Overall, sequences were highly conserved at positions -2 (>99.9% C), -1 (>81.6% A), 0 (>73.7% R), n (>77.6% D), n + 1 (>58.8% Y), and n + 2(99.7% W) (Figure 1A). The extracted structures were categorized into (C+)-bulges (34%)—similar in structure to an antiparallel G1 bulge with a hydrogen bond from the n + 1amide to the carbonyl at the 0 position (based on NH-OC distances of less than 2.75 Å)—and (C-)-bulges (66%) lacking the third bulge hydrogen bond. Further clustering based on backbone structure revealed six main subclusters of bulge-like conformations presenting subtle structural variations (Figures S3-S9). According to our Ramachandran plot analysis (Figure 1B), the backbone conformational space of the main bulge residues is fairly constant across all CDR-H3 structures, with position 0 mostly populating the polyproline type-II region, position *n* populating both γ' or α -regions, and position n + 1 mostly populating the β -region. Strikingly, the last two CDR-H3 loop residues, also pertaining to the bulge at positions n-1 and n occupied γ' or α_L basins, and δ or α basins respectively, illustrating a significant conformational variability imparted by the twisted geometry of β -bulges (Figure 1C). 41,42 In addition, this analysis revealed that these vicinal residues (n, n + 1) adopt unusual conformations similar to an inverse NHN γ -turn with the NH(n + 1) hydrogenbonded perpendicular to the acceptor lone pair N at position n

and to the side-chain carbonyl forcing residue n into a bridge conformation between γ' - and $\alpha_{\rm L}$ -regions. ⁴³,⁴⁴

Our structural analysis revealed that the typical 3-residue kinked base of bulges (noted in magenta: 0, n, n + 1) plays a significant role in stabilizing CDR-H3s. In addition to the characteristic bifurcated hydrogen bond pattern of the β -bulge base between positions 0, n, and n + 1, conserved interactions consist of a salt bridge between positions 0 and n and cation $-\pi$ interactions between 0 and n + 1 (~5.0 Å) (Figure 1C,D). More importantly, additional residues on the opposite face of the bulge base (positions -1, n-1 and n+2, noted in blue) are clearly contributing to extend the flanks of the bulge. $CH-\pi$ interactions between -1 and n-1 and the tryptophan at n + 2 (both ~ 4.0 Å) and a hydrogen bond between the n -1 carbonyl and the n + 2 tryptophan side-chain NH_E appear to further stabilize the kinked backbone to help connect the H3 loop conformation to its stem. However, the conformational dispersion observed across the twisted backbone (n-1, n, n+1)1) likely reflects that CDR-H3 topologies are intimately linked to additional stabilizing interactions with other CDRs and the antibody framework itself. This finding raises the intriguing question that which of these structural features are preserved in CDR-H3 scaffolds outside of the native antibody context. To replicate the intricate structures of CDR-H3s into folded and thermally stable short scaffolds, a screening of biomimetic constructs was deemed necessary. As shown in the archetypal (C-)-bulge motif of pembrolizumab (PDB code: 5B8C), we hypothesized that a number of weak attractive noncovalent interactions including a CH/π interaction between proximal A(0):W(n + 2), a $R^+(0):D^-(n)$ salt bridge potentially associated with a π -salt stacking from the Y(n + 1) aromatic side chain, and an intramolecular side-chain hydrogen bond W(n + 2):F(n - 1) could be collectively implicated to stabilize the structural kinked base of these β -bulges.⁴⁵

Engineering a Library of Standalone β -Hairpin Peptide Mimics of Bulged CDR-H3. To test this hypothesis and identify a de novo synthetic β -hairpin mimic of a CDR-H3 (C-)-bulge, we carried out the synthesis of a peptide library 1a-l using a typical Fmoc-chemistry on solid support (Table inset in Figure 2A). As a proof-of-principle, we selected the CDR-H3 apex of pembrolizumab (Figure 1D) to design our bulged hairpin mimics. The native sequence excised from pembrolizumab was initially capped by a short stabilizing RW···WE motif in 1a, but this peptide was shown by CD spectroscopy to be fully unfolded (vide infra). 46 As a control, a synthetic coil model 1b of a similar primary sequence was also prepared to calibrate the unfolded baseline required for CDmelts analysis. Within this peptide library, most analogs 1a-j and 11 possess a modified 10-residue loop (F10G) to enhance solubility, while peptide 1k mimics an additional example of CDR-H3 loop excised from the GY-14 antibody (PDB code

Specific substitutions (lysine/valine: A4(K/V), phenylalanine/N-methyl-tryptophan: W17(F/ $^{\rm Me}$ W), and asparagine: D15N were incorporated into our design to probe the noncovalent interactions within the extended structure around the bulge of CDR-H3s. A major hurdle in producing acyclic hairpins is often associated with the entropic penalty of long-loop nucleation (>10-residue); therefore, we incorporated a β -strap RWV···(V/H)WE developed by our group to strengthen the hairpin scaffold. This approach capitalized on a salt bridge at the hairpin termini following a tryptophan zipper-like stabilizing W/W interaction and a hydrophobic packing pair

V/(V/H) in place of the original CDR-H3 C^{96}/G^{111} pair. This strap technology affords enthalpic stability required to rigidify the N- and C-hairpin termini and minimize any undesired fraying. The length of the strap proved to be crucial to enabling a relatively high %-folding of each peptide in a two-stranded β -hairpin conformation required for studying the CDR-H3 motif. Initial results demonstrated that the V3/V18 pair was more efficient in structuring these hairpins (see Figure 2, inset Table, 1d vs 1e) and was therefore carried on throughout the study. As a control, a "regular" (nonbulged) [10:12]-hairpin 1l was prepared with a similar strap to contrast the folding properties of bulge-like analogues by CD and NMR spectroscopy.

Tertiary Structure and Thermal Stability of CDR-H3 β -Hairpin Mimics Evaluated by CD Spectroscopy. To evaluate the impact of various (C-)-bulge sequences on the global hairpin stability by CD spectroscopy, we specifically modified residues at the -1, n, and n + 2 positions. The crossstrand pair of tryptophans W2/W19 close to the N-/C- strap termini creates a characteristic and very intense exciton couplet maxima at 212 and 228 \pm 1 nm in the far-UV CD spectra of β hairpins (negative/positive maxima from $\pi - \pi^*$ transition).⁴⁹ This spectroscopic probe positioned nearby the hairpin termini can be exploited to rapidly and reliably rank the stability of hairpins 1c-l in water (Table inset in Figure 2A). Regrettably, the poor solubility of hairpin 1c in water affected the folding results thus requiring the addition of MeOH (10% vol/vol). To circumvent this issue, a F10G substitution was designed at the center of the H3 loop sequence in hairpins 1d-j to reduce hydrophobicity, while affording additional flexibility to the loop. Strikingly, a unique positive CD band at 202 \pm 2 nm was observed on each hairpin spectra with varying intensity except for the "regular" hairpin 11 and the unfolded peptide 1j (Figure 2B). CD-spectra were also deconvoluted to determine individual elements of secondary structure using BeStSel. 50 The results converged to suggest that the positive Cotton effect at 202 \pm 2 nm (Figure 2B) corresponds a right-handed twist of an antiparallel β -sheet which may conceivably be imparted by a kinked structure as seen in β -bulge structures (SI, Figures S9-16). In addition, the thermal denaturation of these acyclic hairpins 1c-l was performed from 0 to 95 °C by monitoring the disappearance of both bands at 202 and 228 nm corresponding to the local kinked, bulge-like conformation and the hairpin termini, respectively (Figure 2C). CD-melts were computed by fitting the ellipticity intensity decay as a function of temperature $[\theta(T)]_{202/228}$ to the thermodynamic Gibbs-Helmholtz equation for a two-state model of transition $(\Delta C_p \neq 0$, see thermodynamic data SI, Table S3).⁵¹ With the exception of 1c, the unfolded analog 1j and hairpin 1k from a different CDR-H3 loop, all bulge-like mimics were highly folded ($\chi_{\rm F} \geq 65\%$ at 18 °C) and structurally stable hairpins with melting temperatures (T_m) largely exceeding physiological temperature. To compare stability more accurately across this series of hairpins (single AA substitution per sequence), we performed a simultaneous global fit of melting curves (Figure 2A, see SI, Figure S32 and Table S5). Noticeably, the D15N substitution in 1f had a profound destabilizing effect. This result suggests that the R5:D15 ionic interaction might contribute to the stability of the bulge-like structures as previously proposed by Nakamura.³² In stark contrast, both A4K and A4 V substitutions in hairpins 1g and 1h, respectively, afforded a substantial gain of stability above physiological temperature (T_m upshift), which led to a thermostable hairpin behavior (Figure 2D, SI Table S5). The

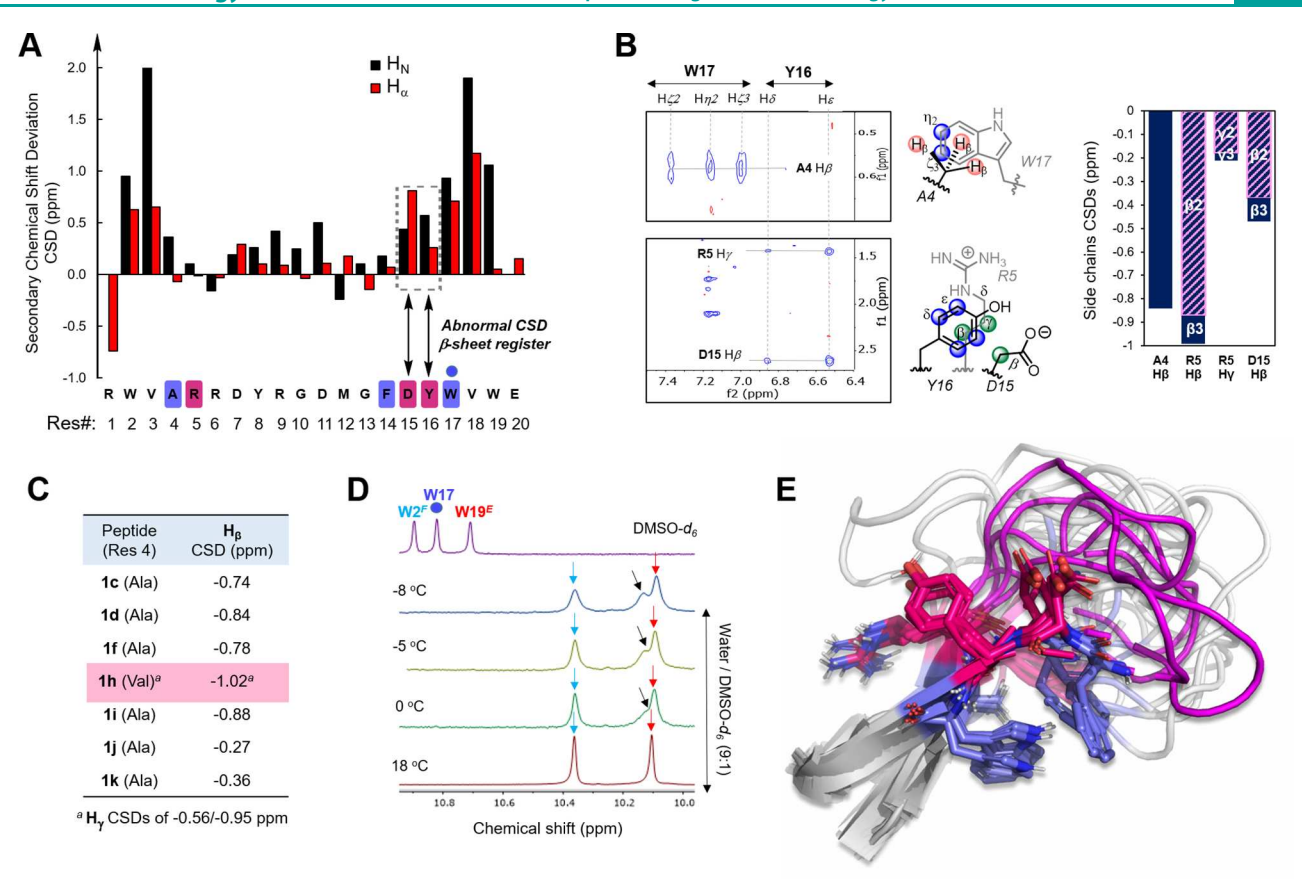


Figure 3. NMR structure of a bulge-like CDR-H3 β -hairpin mimic in aqueous solution. (A) Backbone amide H_N and H_α chemical shift deviations (CSDs) for hairpin 1d, highlighting a downfield abnormality at the bulge D15:Y16 residues. (B) Strip cross sections through the NOESY spectrum of hairpin 1d locating the A4:W17 and [R5,D15]:Y16 long-range correlations through space (left), along with the most significant side-chain CSD values for these residues. (C) upfield CSDs recorded for the bulge residue 4 (A/V), reflecting a CH- π shielding interaction created by W17. (D) Overlay of ¹H NMR traces revealing the W17(H_{ε1}) signal line broadening with the temperature indicative of a weak intramolecular hydrogen bond in 1d. (E) Dynamic structure of the bulged-like hairpin 1d in solution (PDB code: 8W0Q). Overlay of the five main conformer populations representative of the global 20-state ensemble of 1d elucidated by NMR spectroscopy and computational modeling with the stabilizing terminal β -strap (gray side chains) and the kinked/extended base of the β -bulge-like structure (magenta/blue).

flatter slopes of CD-melts observed for 1g and 1h below 30 °C and at $T_{\rm m}$ demonstrate the benefit of sturdier bulge-like motifs on the global hairpin unfolding. Denaturation experiments additionally support that the lack of cooperativity between the kinked and stem segments of β -hairpins improves their overall thermal stability. To probe the importance of the A4:W17 interaction, two substitutions W17F $\bar{\mbox{(in 1j)}}$ and W17 ^{Me}W (in 1i) were evaluated. The first W17F substitution completely prevented the hairpin formation of 1j yielding a random coil structure, therefore demonstrating that a bulge-like fold is greatly dependent on the W17 indole side-chain. Second, the W17^{Me}W modification designed to suppress any potential sidechain H-bond also largely affected the denaturation curve of hairpin 1i with a loss of about 20%-folding throughout the entire range of temperature (e.g., 1i vs 1d, $\Delta\Delta G^{\circ}$ of +0.4 kcal/ mol). These results are in full agreement with the NMR data (vide infra, Figure 3B-C) supporting the notion that the W17 residue plays a pivotal role in the kinked bulge-like structure through hydrogen bonding and a CH/ π interaction with A4.

To further probe the stability of these hairpins, a pH acidification (6.5–2.2) was used to induce an acid-mediated denaturation. Unlike the regular hairpin 11 which is fully unfolded at such acidic pH, the kinked hairpins 1c–k were noticeably less affected (at the exception of 1e and 1k bearing an acid-labile histidine in the strap, SI Figure S30, Table S4).

Despite the fact that the CD-band at 202 nm disappeared at this low pH, the overall hairpin folds remained exceptionally high ($\chi_{\rm F}$ 60–80%) with $T_{\rm m}>$ 30 °C, thus highlighting the promise of engineering highly structured CDR-H3 peptide mimetics. In addition, the CD-study demonstrates that the kinked, bulge-like motifs of CDR-H3s can be easily identified by their intense spectroscopic signature at 202 \pm 2 nm. Overall, kinked β -hairpins 1d-i are better folded than the regular benchmark hairpin 11 ($\Delta\chi_{\rm F}>$ 10–20%). These results indicate that a biomimetic design incorporating bulge motifs at the edge of a long H3 loop can deliver highly structured β -hairpins.

Structural Characterization and Dynamic Conformational Ensemble Determination of a Standalone CDR-H3 Peptide Mimic. To elucidate the structural features of our original CDR-H3 model, 1 H, TOCSY, 1 H $-^{13}$ C HSQC, and 1 H $-^{1}$ H NOESY NMR spectra were recorded for hairpin 1d in water containing small amounts of DMSO- d_6 (90:10 vol/vol) to increase solubility. As shown in Figure 3A, the secondary chemical shift deviations (CSDs) from both backbone H_N and H $_{\alpha}$ signals in the R 1 WVAR...YWVWE 20 sequence revealed a typical pattern of β -sheet register flanking the 10-residue [RDYRGDMGFD] loop. These data are essentially consistent with a [10:12]-hairpin fold. Of importance, both H_N and H $_{\alpha}$ CSDs of residues D15 and Y16 in hairpin 1d were abnormally

high (0.25-0.70 ppm, Figure 3A). This notable stereoelectronic effect, presumably imparted by the presence of a kinked, bulge-like structure, prompted us to further examine the key side-chain interactions between each residue (Figure 3B). We found that the β - and γ -hydrogen signals on both R5 and D15 residues experienced significant upfield shifts (CSDs of -0.47 to -0.76 ppm) presumably due to a shielding effect of the facing Y16 aromatic ring. This interpretation was confirmed by a set of medium to strong long-range NOESY correlations between Y16(H_{δ/ϵ}) and both R5(H_{β}) and D15(H_{β}), suggesting that these three residues are in close contact interactions around the Y16 π -system (Figure 3B).⁵³ These results are in line with the cation- π and bridge salt interactions found in the kinked base of the pembrolizumab β bulge (AAs in magenta Figures 1D and 3E). In addition, the sheer broadness of the $A4(H_{\beta})$ resonance (restricted conformational ensemble in slow equilibrium on the NMR time scale) and its significant CSD of -0.84 ppm are evidence of a profound shielding interaction (Figure 3B,C). This would be consistent with a close contact CH/π interaction between A4 and W17 that is otherwise supported by several strong long-range NOESY correlations between W17(H_{$\zeta3/\eta2$}) and $A4(H_{\beta})$. S4-56 The large CSD of $A4(H_{\beta})$ was further observed across the entire series of bulge-like hairpins (Figure 3C). While all alanine-derived motifs presented a similar chemical shift deviation of the A4H $_{\beta}$ signals (-0.74 to -0.88 ppm), the valine of 1h endured a greater shielding effect of 1.02 ppm in addition to the H_{γ} CSDs of -0.56 and -0.95 ppm. These results are consistent with a more compactly folded structure. In comparison, smaller CSDs were recorded for the $A4(H_{\beta})$ resonances of a weakly folded hairpin 1k (-0.35 ppm) and the random coil 1j (vide supra CD section). Interestingly, the unfolded nature of 1j strongly suggests that a tryptophan at position 17 is essential for structuring the CDR-H3 mimics. Tryptophan side-chain NH_{ϵ_1} signals are typically sharp peaks resonating at 10.0–10.5 ppm. These features were observed for both edge-to-face interacting tryptophan W2^F/W19^E within the strap segment of 1d, but W17($H_{\varepsilon 1}$) was hardly seen on ${}^{1}H$ NMR spectra in the range of temperature studied (Figure 3D). Such abnormal peak broadening observed for the W17(H_{E1}) signal is a hallmark of interconverting conformers in a slowexchange regime on the NMR time scale. Due to the emergence of this signal at low temperature, we can speculate that the W17 side chain is conformationally restricted by a weak intramolecular hydrogen bond. One possibility could be a hydrogen bond between W17 and F14 following the pattern observed in most crystal structures of bulged CDR-H3s (F(n -1):W(n + 2), Figure 1D).

To further probe the stability and dynamic properties of these bulge-like hairpins, both amide-NH temperature coefficients ($\Delta\delta H_{\rm N}/\Delta T$) and hydrogen—deuterium exchange rates ($k_{\rm H/D}$) were measured in 1d by NMR spectroscopy. H/D-exchange experiments can in principle probe both open and closed populated conformational states of hairpins in solution to help distinguish topologies between loop, strap, and kinked bulge-like sequences (SI, Figure S34 and Table S14).⁵⁷ The H/D-exchange experiment confirmed the presence of several strong H-bonds within the strap such as the pair of valines V3/V18 ($k_{\rm H/D}$ < 1.4 × 10⁻³ min⁻¹) and the terminal E20 residue ($k_{\rm H/D}$ of 6.8 × 10⁻³ min⁻¹). More interestingly, the amide $k_{\rm H/D}$ value of 33.5 × 10⁻³ min⁻¹ for the F14 bulge residue, although relatively rapid, remains in the expected range for a weak hydrogen bond. To confirm whether these backbone amides

are involved in intramolecular hydrogen bonds, amide-H_N temperature coefficients $(\Delta \delta H_N/\Delta T)$ were measured from variable temperature ¹H NMR spectra (SI, Table S13). It is well established that solvent-protected and/or hydrogenbonded amide protons typically have a $\Delta \delta H_N/\Delta T \geq -4.6$ ppb/K.⁵⁸ As anticipated from the H/D exchange rates, the temperature coefficients recorded for both V3/V18 (-15.2ppb/K) and E20 (-6.0 ppb/K) are suggestive of weak Hbonds within the strap. The abnormally high temperature coefficients for the V3/V18 pair have been previously reported for amides transiently hydrogen-bonded among rapidly equilibrating conformers, thus suggesting that the acyclic hairpin 1d equilibrates between open and closed forms over the range of temperature studied. 59,60 Furthermore, the amides-H_N of R5 and F14 with $\Delta \delta H_N/\Delta T$ of -5.3 and -5.7 ppb/K, respectively, were also found to participate in weakly persisting hydrogen bonds. R5 at position 0 could form a hydrogen bond across the hairpin with D15(n) and/or Y16(n+ 1) consistent with a bulge-like structure. On the other hand, persistent backbone hydrogen bonding of F14(n-1) position may indicate residual structures in what may otherwise be assumed to be a disordered loop.

Finally, a 3D-conformational ensemble of hairpin 1d in solution at 298 K was modeled based on NMR chemical shifts (1H, 13C, and 15N), NOESY correlations (including >40 longrange interactions), and $^{3}J_{HN-H\alpha}$ backbone and $^{3}J_{H\alpha-H\beta}$ sidechain coupling constants. Briefly, a large initial ensemble of 10 million plausible conformers was generated via simulated annealing with the CHARMM c36m force field followed by explicit solvent molecular dynamics simulations under NOE and backbone torsion angle restraints (see SI). The initial ensemble was reduced to a subset of 60,000 stereochemically most ideal conformers. From these, 20 conformers were extracted within a maximum-entropy framework to obtain a maximal agreement between the model and the experimental ensemble-averaged NOE distances and *I*-coupling values (see SI). In this ensemble refinement process, conformer selection and assignment of weights were iteratively optimized to closely represent the true dynamic ensemble of the underlying experimental NMR data. It is readily apparent that the conformational ensemble (Figure 3E) consists of a highly ordered hairpin terminal β -strap, flanked by mostly kinked configurations that resemble the bulge conformations seen in the CDR-H3 structures, and a more disordered loop for the remaining residues. This allows the conclusion that our truncated CDR-H3 mimic 1d is a well-folded hairpin that retains the overall structural features seen in the crystal structures of antibodies. However, a more detailed analysis of specific features around the residues forming the β -bulge revealed some major differences (Figure 4). The classic β bulge backbone hydrogen pattern is incomplete with the n:0 hydrogen bond present in only a subset of conformers (Figure 4A). Nevertheless, residues R5(0)/D15(n)/Y16(n+1) are on the same face of the hairpin and in close proximity, forming a kinked base as in CDR-H3 bulges. However, the R5:D15 salt bridge interaction was missing from all conformers. Instead, R5 is found bent over the hairpin strap to interact with the Cterminal E20. Because R5 is oriented away from D15, the cation- π interaction is also weakened in the hairpin ensemble (Figure 4A). CH/ π contacts from W17(n + 2) to F14(n - 1) and A4(-1) are similarly close in about half of 1d conformers, while the W17-NH ε hydrogen bond to the F14 backbone carbonyl, consistent with the extended bulge architectures, is

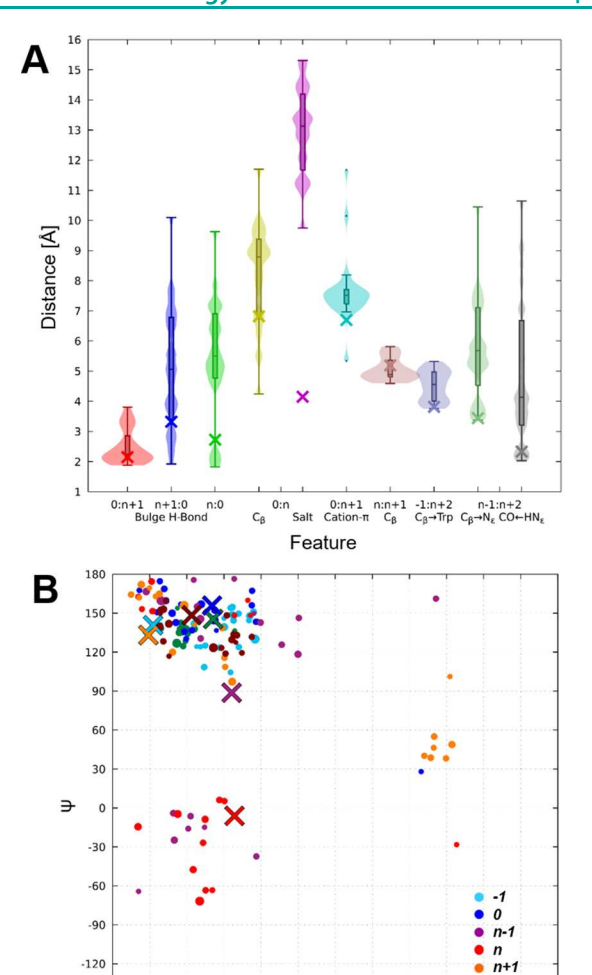


Figure 4. 3D-Features of the de novo CDR-H3 β-hairpin mimetic 1d (20-state ensemble). (A) Violin plots indicating the distribution of structural features as in Figure 1C for bulge-like residues within the CDR-H3 mimic. (B) Backbone Ramachandran analysis of kink residues. Values from the parental pembrolizumab (PDB: 5B8C) are indicated with '×' marks and dot size reflects conformer weight.

120 150

90

only present in some conformations. Instead, there is a close interaction within the loop between the F14 backbone carbonyl and the backbone amide of M12. This observation is consistent with the amide- H_N temperature coefficient analysis described above that suggests that F14 carbonyl is involved in hydrogen bonding. Overall, the distribution of backbone Ramachandran angles for the solution ensemble of 1d is relatively broad, indicating significant conformational dynamics (Figure 4B). However, the distributions are analogous to CDR-H3 structures and the values for pembrolizumab. Most notably, residues at positions n-1 and n sample the α_L/γ_T and α -regions of the Ramachandran map forming the expected twisted conformation of bulges.

CONCLUSIONS

-150

-180 -150 -120

-90 -60

Known CDR-H3 structures fall into tightly clustered kinked and extended conformations, with a kinked (C+) or (C-) bulge conformation around the consensus sequence AR-loopFD-YW being the most prominent motif. According to

our analysis, the classic three-residue bulge definition (0, n, n + 1) extends to a six-residue motif in CDR-H3s due to additional highly conserved and stabilizing noncovalent interactions between positions -1, n-1, and n+2. Presumably, the conserved six-residue motif provides the stability and versatility necessary to display a wide variety of loops adaptable to distinct antigens.

We demonstrate here that the key CDR-H3 motif can be synthetically crafted into short yet stable standalone β -hairpin scaffolds that retain most structural features of the parental CDR-H3s outside the antibody context. The pH- and thermally induced denaturation studies support the notion that CDR-H3 mimics are intrinsically stable yet conformationally flexible, curbing the cooperativity between the β -sheet and loop segments to enhance the global hairpin stability. Our results also suggest that the presence of a bulge-like kinked structure can be identified via CD spectroscopy by a unique signature band at 202 ± 2 nm allowing for a rapid and general characterization of CDR-H3-like structures. The biomimetic A(-1)V substitution—naturally occurring in CDR-H3 sequences—yielded the most stable bulged-like β -hairpin 1h ($T_{\rm m}$ of 70 °C, 85%-folding at physiological temperature), which is significantly superior to the regular benchmark hairpin 11.

A full characterization of the pembrolizumab mimic 1d by NMR spectroscopy revealed a structural ensemble with a rigid β -sheet stem and kinked bulge-like motif affording significant conformational flexibility toward the loop (PDB code: 8W0Q). In the NMR ensemble, the combination of strong CH/π interaction and weaker intramolecular hydrogen bond created by the W(n + 2) side chain strongly suggests that this highly conserved residue is essential to the bulge architecture of the kinked CDR-H3 motifs. However, we also identify some differences between the NMR ensemble of 1d and the original pembrolizumab crystal structure such as the apparent lack of a salt bridge between R5 and D15. Differences due to the more dynamic nature of the standalone hairpin may be expected as the antibody framework certainly constrain the native CDR-H3 conformational space. The lack of NMR evidence characterizing the proximity of the R5:D15 interaction might be due to the dynamic nature of the conformational ensemble. Other reasons may be imparted by the synthetic construct 1d itself such as the terminal E20 residue interaction to R5. By replacing E20 by a nonacidic residue, it is conceivable that the R5:D15 salt bridge could be restored like in typical (C-) bulges. Further studies will be needed to fully understand how the detailed structure of CDR-H3 mimics may vary from their parental structures as a function of primary amino acid sequences.

The structural insights gained into CDR-H3 architectures represent an important step to assist the development of therapeutic antibodies and future loop designs for high-throughput screening by (phage- and mRNA-) display technologies. Given the uniqueness of CDR-H3 loops in ultralong CDRs⁶¹ and other broad neutralizing antibodies, ^{62,63} we anticipate that having access to bulge-like CDR-H3 mimics will greatly facilitate future structural studies, providing valuable tools to probe H3 loop rigidification and conformational dynamics in the context of antibody drug development. ⁶⁴

ASSOCIATED CONTENT

5 Supporting Information

The Supporting Information is available free of charge at https://pubs.acs.org/doi/10.1021/acschembio.4c00236.

Experimental procedures and analytical data for all β -hairpin peptides, variable temperature CD and NMR data, H/D exchange for hairpin 1d, and computational modeling protocols (PDF)

Raw CD-data and denaturation curves (XLSX)
Data-derived 3D-structure ensemble of 1d (PDB)

AUTHOR INFORMATION

Corresponding Authors

Michael Feig — Department of Biochemistry and Molecular Biology, Michigan State University, East Lansing, Michigan 48824, United States; orcid.org/0000-0001-9380-6422; Email: mfeiglab@gmail.com

Stéphane P. Roche — Department of Chemistry and Biochemistry, Florida Atlantic University, Boca Raton, Florida 33431, United States; orcid.org/0000-0002-3019-2168; Email: sroche2@fau.edu

Authors

Guangkuan Zhao – Department of Chemistry and Biochemistry, Florida Atlantic University, Boca Raton, Florida 33431, United States

Alexis D. Richaud – Department of Chemistry and Biochemistry, Florida Atlantic University, Boca Raton, Florida 33431, United States

R. Thomas Williamson — Department of Chemistry and Biochemistry, University of North Carolina Wilmington, Wilmington, North Carolina 28409, United States; orcid.org/0000-0001-7450-3135

Complete contact information is available at: https://pubs.acs.org/10.1021/acschembio.4c00236

Author Contributions

This project was conceived by S.P.R. and M.F.; G.Z., A.D.R., and R.T.W. performed the research experiments and data analysis. M.F. designed the computational aspects of this study and generated the computational 3D-model of hairpin 1d based on NMR data obtained by A.D.R., G.Z., and R.T.W. The manuscript was written through contributions of S.P.R. and M.F.; All authors have given approval to the final version of the manuscript.

Notes

The authors declare no competing financial interest. PDB code: 8W0Q.

■ ACKNOWLEDGMENTS

We are grateful for the financial support from the National Institutes of Health (NIGMS Grant: R21GM132754 to S.P.R., G.Z., and A.D.R.; NIGMS Grant R35GM126948 to M.F.).

ABBREVIATIONS

Ag antigen Ab antibody

CDR complementarity-determining region

CSD chemical shift deviation
TOCSY total correlation spectroscopy

HSQC heteronuclear single quantum coherence spectrosco-

NOESY nuclear Overhauser effect spectroscopy

REFERENCES

- (1) Wedemayer, G. J.; Patten, P. A.; Wang, L. H.; Schultz, P. G.; Stevens, R. C. Structural Insights into the Evolution of an Antibody Combining Site. *Science* **1997**, *276*, 1665.
- (2) Khass, M.; Vale, A. M.; Burrows, P. D.; Schroeder, H. W., Jr The sequences encoded by immunoglobulin diversity (DH) gene segments play key roles in controlling B-cell development, antigenbinding site diversity, and antibody production. *Immunol. Rev.* **2018**, 284, 106.
- (3) Glanville, J.; Zhai, W.; Berka, J.; Telman, D.; Huerta, G.; Mehta, G. R.; Ni, I.; Mei, L.; Sundar, P. D.; Day, G. M. R.; Cox, D.; Rajpal, A.; Pons, J. Precise determination of the diversity of a combinatorial antibody library gives insight into the human immunoglobulin repertoire. *Proc. Natl. Acad. Sci. U.S.A.* **2009**, *106*, 20216.
- (4) (a) Wong, S. E.; Sellers, B. D.; Jacobson, M. P. Effects of somatic mutations on CDR loop flexibility during affinity maturation. *Proteins* **2011**, 79, 821.
- (5) Schmidt, A. G.; Xu, H.; Khan, A. R.; O'Donnell, T.; Khurana, S.; King, L. R.; Manischewitz, J.; Golding, H.; Suphaphiphat, P.; Carfi, A.; Settembre, E. C.; Dormitzer, P. R.; Kepler, T. B.; Zhang, R.; Moody, M. A.; Haynes, B. F.; Liao, H.-X.; Shaw, D. E.; Harrison, S. C. Preconfiguration of the antigen-binding site during affinity maturation of a broadly neutralizing influenza virus antibody. *Proc. Natl. Acad. Sci. U.S.A.* 2013, 110, 264.
- (6) Klein, F.; Diskin, R.; Scheid, Johannes F.; Gaebler, C.; Mouquet, H.; Georgiev, I. S.; Pancera, M.; Zhou, T.; Incesu, R.-B.; Fu, Brooks Z.; Gnanapragasam, Priyanthi N. P.; Oliveira, Thiago Y.; Seaman, Michael S.; Kwong, Peter D.; Bjorkman, Pamela J.; Nussenzweig, Michel C. Somatic Mutations of the Immunoglobulin Framework Are Generally Required for Broad and Potent HIV-1 Neutralization. *Cell* **2013**, *153*, 126.
- (7) (a) DeKosky, B. J.; Lungu, O. I.; Park, D.; Johnson, E. L.; Charab, W.; Chrysostomou, C.; Kuroda, D.; Ellington, A. D.; Ippolito, G. C.; Gray, J. J.; Georgiou, G. Large-scale sequence and structural comparisons of human naive and antigen-experienced antibody repertoires. *Proc. Natl. Acad. Sci. U. S. A.* **2016**, *113*, No. E2636.
- (8) Jeliazkov, J. R.; Sljoka, A.; Kuroda, D.; Tsuchimura, N.; Katoh, N.; Tsumoto, K.; Gray, J. J. Repertoire Analysis of Antibody CDR-H3 Loops Suggests Affinity Maturation Does Not Typically Result in Rigidification. *Front. Immunol.* **2018**, *9*, 413.
- (9) Yin, J.; Mundorff, E. C.; Yang, P. L.; Wendt, K. U.; Hanway, D.; Stevens, R. C.; Schultz, P. G. A Comparative Analysis of the Immunological Evolution of Antibody 28B4. *Biochemistry* **2001**, *40*, 10764
- (10) Bozhanova, N. G.; Sangha, A. K.; Sevy, A. M.; Gilchuk, P.; Huang, K.; Nargi, R. S.; Reidy, J. X.; Trivette, A.; Carnahan, R. H.; Bukreyev, A.; Crowe, J. E.; Meiler, J. Discovery of Marburg virus neutralizing antibodies from virus-naive human antibody repertoires using large-scale structural predictions. *Proc. Natl. Acad. Sci. U.S.A.* 2020, 117, 31142.
- (11) Fernández-Quintero, M. L.; Loeffler, J. R.; Bacher, L. M.; Waibl, F.; Seidler, C. A.; Liedl, K. R. Local and Global Rigidification Upon Antibody Affinity Maturation. *Front. Mol. Biosci.* **2020**, *7*, 182.
- (12) Vajda, S.; Porter, K. A.; Kozakov, D. Progress toward improved understanding of antibody maturation. *Curr. Opin. Struct. Biol.* **2021**, 67, 226.
- (13) Favre, M.; Moehle, K.; Jiang, L.; Pfeiffer, B.; Robinson, J. A. Structural Mimicry of Canonical Conformations in Antibody hypervariable Loops Using Cyclic Peptides Containing a Heterochiral Diproline Template. *J. Am. Chem. Soc.* **1999**, *121*, 2679.
- (14) Decanniere, K.; Muyldermans, S.; Wyns, L. Canonical antigenbinding loop structures in immunoglobulins: more structures, more canonical classes? *J. Mol. Biol.* **2000**, *300*, 83.

- (15) North, B.; Lehmann, A.; Dunbrack, R. L. A New Clustering of Antibody CDR Loop Conformations. J. Mol. Biol. 2011, 406, 228.
- (16) Chang, H.-J.; Jian, J.-W.; Hsu, H.-J.; Lee, Y.-C.; Chen, H.-S.; You, J.-J.; Hou, S.-C.; Shao, C.-Y.; Chen, Y.-J.; Chiu, K.-P.; Peng, H.-P.; Lee, Kuo H.; Yang, A.-S Loop-Sequence Features and Stability Determinants in Antibody Variable Domains by High-Throughput Experiments. *Structure* **2014**, *22*, 9.
- (17) Breden, F.; Lepik, C.; Longo, N. S.; Montero, M.; Lipsky, P. E.; Scott, J. K. Comparison of Antibody Repertoires Produced by HIV-1 Infection, Other Chronic and Acute Infections, and Systemic Autoimmune Disease. *PLoS One* **2011**, *6*, No. e16857.
- (18) Chothia, C.; Lesk, A. M.; Tramontano, A.; Levitt, M.; Smith-Gill, S. J.; Air, G.; Sheriff, S.; Padlan, E. A.; Davies, D.; Tulip, W. R.; Colman, P. M.; Spinelli, S.; Alzari, P. M.; Poljak, R. J. Conformations of immunoglobulin hypervariable regions. *Nature* 1989, 342, 877.
- (19) Wong, W. K.; Leem, J.; Deane, C. M. Comparative Analysis of the CDR Loops of Antigen Receptors. *Front. Immunol.* **2019**, *10*, 2454.
- (20) (a) Sela-Culang, I.; Alon, S.; Ofran, Y. A Systematic Comparison of Free and Bound Antibodies Reveals Binding-Related Conformational Changes. *J. Immunol.* **2012**, *189*, 4890.
- (21) Fernández-Quintero, M. L.; Loeffler, J. R.; Kraml, J.; Kahler, U.; Kamenik, A. S.; Liedl, K. R. Characterizing the Diversity of the CDR-H3 Loop Conformational Ensembles in Relationship to Antibody Binding Properties. *Front. Immunol.* **2019**, *9*, 3065.
- (22) Kado, Y.; Mizohata, E.; Nagatoishi, S.; Iijima, M.; Shinoda, K.; Miyafusa, T.; Nakayama, T.; Yoshizumi, T.; Sugiyama, A.; Kawamura, T.; Lee, Y.-H.; Matsumura, H.; Doi, H.; Fujitani, H.; Kodama, T.; Shibasaki, Y.; Tsumoto, K.; Inoue, T. Epiregulin Recognition Mechanisms by Anti-epiregulin Antibody 9E5. J. Biol. Chem. 2016, 291, 2319.
- (23) Kunik, V.; Ofran, Y. The indistinguishability of epitopes from protein surface is explained by the distinct binding preferences of each of the six antigen-binding loops. *Protein Eng. Des. Sel.* **2013**, 26, 599.
- (24) (a) Kuroda, D.; Shirai, H.; Jacobson, M. P.; Nakamura, H. Computer-aided antibody design. *Prot. Eng. Des. Sel.* **2012**, *25*, 507.
- (25) Tsuchiya, Y.; Mizuguchi, K. The diversity of H3 loops determines the antigen-binding tendencies of antibody CDR loops. *Protein Sci.* **2016**, *25*, 815.
- (26) Fernández-Quintero, M. L.; Kraml, J.; Georges, G.; Liedl, K. R. CDR-H3 loop ensemble in solution conformational selection upon antibody binding. *mAbs* **2019**, *11*, 1077.
- (27) Weitzner, B. D.; Kuroda, D.; Marze, N.; Xu, J.; Gray, J. J. Blind prediction performance of RosettaAntibody 3.0: Grafting, relaxation, kinematic loop modeling, and full CDR optimization. *Proteins* **2014**, 82, 1611.
- (28) Sevy, A. M.; Meiler, J. Antibodies: Computer-Aided Prediction of Structure and Design of Function *Microbiol. Spectr.* 2014, 2.
- (29) Weitzner, B. D.; Dunbrack, R. L.; Gray, J. J. The Origin of CDR H3 Structural Diversity. *Structure* **2015**, 23, 302.
- (30) Finn, J. A.; Koehler Leman, J.; Willis, J. R.; Cisneros, A., III; Crowe, J. E., Jr.; Meiler, J. Improving Loop Modeling of the Antibody Complementarity-Determining Region 3 Using Knowledge-Based Restraints. *PLoS One* **2016**, *11*, No. e0154811.
- (31) Marks, C.; Deane, C. M. Antibody H3 Structure Prediction. Comput. Struct. Biotechnol. J. 2017, 15, 222.
- (32) (a) Shirai, H.; Kidera, A.; Nakamura, H. Structural classification of CDR-H3 in antibodies. FEBS Lett. 1996, 399, 1.
- (33) Morea, V.; Tramontano, A.; Rustici, M.; Chothia, C.; Lesk, A. M. Conformations of the third hypervariable region in the VH domain of immunoglobulins. *J. Mol. Biol.* **1998**, *275*, 269.
- (34) Shirai, H.; Kidera, A.; Nakamura, H. H3-rules: identification of CDR-H3 structures in antibodies. *FEBS Lett.* **1999**, 455, 188.
- (35) (a) Richardson, J. S.; Getzoff, E. D.; Richardson, D. C. The beta bulge: a common small unit of nonrepetitive protein structure. *Proc. Natl. Acad. Sci. U.S.A.* **1978**, *75*, 2574.
- (36) Chan, A. W. E.; Hutchinson, E. G.; Harris, D.; Thornton, J. M. Identification, classification, and analysis of beta-bulges in proteins. *Protein Sci.* 1993, 2, 1574.

- (37) Craveur, P.; Joseph, A. P.; Rebehmed, J.; de Brevern, A. G. β -Bulges: Extensive structural analyses of β -sheets irregularities. *Protein Sci.* **2013**, 22, 1366.
- (38) (a) Tynan, F. E.; Reid, H. H.; Kjer-Nielsen, L.; Miles, J. J.; Wilce, M. C. J.; Kostenko, L.; Borg, N. A.; Williamson, N. A.; Beddoe, T.; Purcell, A. W.; Burrows, S. R.; McCluskey, J.; Rossjohn, J. A T cell receptor flattens a bulged antigenic peptide presented by a major histocompatibility complex class I molecule. *Nat. Immunol.* **2007**, *8*, 268.
- (39) Capraro, D. T.; Roy, M.; Onuchic, J. N.; Gosavi, S.; Jennings, P. A. β -Bulge triggers route-switching on the functional landscape of interleukin-1 β . *Proc. Natl. Acad. Sci. U.S.A.* **2012**, *109*, 1490.
- (40) Bahrami Dizicheh, Z.; Chen, I. L.; Koenig, P. VHH CDR-H3 conformation is determined by VH germline usage. *Commun. Biol.* **2023**, *6*, 864.
- (41) Hollingsworth, S. A.; Karplus, P. A. A fresh look at the Ramachandran plot and the occurrence of standard structures in proteins. *BioMol. Concepts.* **2010**, *1*, 271.
- (42) Porter, L. L.; Rose, G. D. Redrawing the Ramachandran plot after inclusion of hydrogen-bonding constraints. *Proc. Natl. Acad. Sci. U.S.A.* **2011**, *108*, 109.
- (43) Dhar, J.; Kishore, R.; Chakrabarti, P. A novel secondary structure based on fused five-membered rings motif. *Sci. Rep.* **2016**, *6*, 31483.
- (44) Dhar, J.; Kishore, R.; Chakrabarti, P. Delineation of a new structural motif involving NHN γ -turn. *Proteins.* **2020**, 88, 431.
- (45) Salonen, L. M.; Ellermann, M.; Diederich, F. Aromatic Rings in Chemical and Biological Recognition: Energetics and Structures. *Angew. Chem., Int. Ed.* **2011**, *50*, 4808.
- (46) Anderson, J. M.; Kier, B. L.; Shcherbakov, A. A.; Andersen, N. H. An improved capping unit for stabilizing the ends of associated β -strands. *FEBS Lett.* **2014**, *588*, 4749.
- (47) Richaud, A. D.; Zhao, G.; Hobloss, S.; Roche, S. P. Folding in Place: Design of β -Strap Motifs to Stabilize the Folding of Hairpins with Long Loops. *J. Org. Chem.* **2021**, *86*, 13535.
- (48) Cochran, A. G.; Škelton, N. J.; Starovasnik, M. A. Tryptophan zippers: Stable, monomeric β -hairpins. *Proc. Natl. Acad. Sci. U.S.A.* **2001**, *98*, 5578.
- (49) Anderson, J. M.; Kier, B. L.; Jurban, B.; Byrne, A.; Shu, I.; Eidenschink, L. A.; Shcherbakov, A. A.; Hudson, M.; Fesinmeyer, R. M.; Andersen, N. H. Aryl—aryl interactions in designed peptide folds: Spectroscopic characteristics and optimal placement for structure stabilization. *Biopolymers* **2016**, *105*, 337.
- (50) Micsonai, A.; Wien, F.; Kernya, L.; Lee, Y.-H.; Goto, Y.; Réfrégiers, M.; Kardos, J. Accurate secondary structure prediction and fold recognition for circular dichroism spectroscopy. *Proc. Natl. Acad. Sci. U. S. A.* **2015**, *112*, No. E3095.
- (51) Greenfield, N. J. Using circular dichroism collected as a function of temperature to determine the thermodynamics of protein unfolding and binding interactions. *Nat. Protoc* **2006**, *1*, 2527.
- (52) Anderson, J. M.; Andersen, N. H. A pH Switch for β-Sheet Protein Folding. *Angew. Chem., Int. Ed.* **2017**, *56*, 7074.
- (53) Meyer, E. A.; Castellano, R. K.; Diederich, F. Interactions with Aromatic Rings in Chemical and Biological Recognition. *Angew. Chem., Int. Ed.* **2003**, 42, 1210.
- (54) (a) Tatko, C. D.; Waters, M. L. Comparison of C–H··· π and Hydrophobic Interactions in a β -Hairpin Peptide: Impact on Stability and Specificity. *J. Am. Chem. Soc.* **2004**, *126*, 2028.
- (55) Ghosh, P.; Chatterjee, J. CH $-\pi$ interaction between cross-strand amino acid pairs stabilizes β -hairpins. Chem. Commun. 2020, 56, 14447.
- (56) Richaud, A. D.; Mandal, S.; Das, A.; Roche, S. P. Tunable CH/ π Interactions within a Tryptophan Zipper Motif to Stabilize the Fold of Long β -Hairpin Peptides. *ACS Chem. Biol.* **2023**, *18*, 2555.
- (57) Persson, F.; Halle, B. How amide hydrogens exchange in native proteins. *Proc. Natl. Acad. Sci. U.S.A.* **2015**, *112*, 10383.
- (58) Wang, C. K.; Northfield, S. E.; Colless, B.; Chaousis, S.; Hamernig, I.; Lohman, R.-J.; Nielsen, D. S.; Schroeder, C. I.; Liras, S.; Price, D. A.; Fairlie, D. P.; Craik, D. J. Rational design and synthesis of

an orally bioavailable peptide guided by NMR amide temperature coefficients. *Proc. Natl. Acad. Sci. U.S.A.* **2014**, *111*, 17504.

- (59) Andersen, N. H.; Chen, C.; Marschner, T. M.; Krystek, S. R.; Bassolino, D. A. Conformational isomerism of endothelin in acidic aqueous media: a quantitative NOESY analysis. *Biochemistry* **1992**, *31*, 1280.
- (60) Baxter, N. J.; Williamson, M. P. Temperature dependence of 1H chemical shifts in proteins. *J. BioMol. NMR* **1997**, *9*, 359.
- (61) Svilenov, H. L.; Sacherl, J.; Protzer, U.; Zacharias, M.; Buchner, J. Mechanistic principles of an ultra-long bovine CDR reveal strategies for antibody design. *Nat. Commun.* **2021**, *12*, *6737*.
- (62) (a) Willis, J. R.; Finn, J. A.; Briney, B.; Sapparapu, G.; Singh, V.; King, H.; LaBranche, C. C.; Montefiori, D. C.; Meiler, J.; Crowe, J. E. Long antibody HCDR3s from HIV-naïve donors presented on a PG9 neutralizing antibody background mediate HIV neutralization. *Proc. Natl. Acad. Sci. U.S.A.* **2016**, *113*, 4446.
- (63) Sok, D.; Burton, D. R. Recent progress in broadly neutralizing antibodies to HIV. *Nat. Immunol.* **2018**, *19*, 1179.
- (64) Misson Mindrebo, L.; Liu, H.; Ozorowski, G.; Tran, Q.; Woehl, J.; Khalek, I.; Smith; Jessica, M.; Barman, S.; Zhao, F.; Keating, C.; Limbo, O.; Verma, M.; Liu, J.; Stanfield, R. L.; Zhu, X.; Turner, H. L.; Sok, D.; Huang, P.-S.; Burton, D. R.; Ward, A. B.; Wilson, I. A.; Jardine, J. G. Fully synthetic platform to rapidly generate tetravalent bispecific nanobody—based immunoglobulins. *Proc. Natl. Acad. Sci. U. S. A.* 2023, 120, No. e2216612120.